View Article Online
View Journal

# Dalton Transactions

An international journal of inorganic chemistry

## Accepted Manuscript

Postprint of: Lopresti M., Kurowski Ł., Palin L., Milanesio M., Siedzielnik M., Gutmańska K., Dobrenko A., Klimczuk T., Pawelczyk E., Dołęga A., New heterometallic Co/Zn, Ag/Co, and Ag/Zn imidazolates: structural characterization and catalytic activity in the oxidation of organic compounds, DALTON TRANSACTIONS (2024), DOI: 10.1039/D3DT03211F






ROYAL SOCIETY OF CHEMISTRY

rsc.li/dalton

View Article Online
DOI: 10.1039/D3DT03211F

ARTICLE

# New heterometallic Co/Zn, Ag/Co, and Ag/Zn imidazolates: structural characterization and catalytic activity in the oxidation of organic compounds

Received 00th January 20xx,
Accepted 00th January 20xx

DOI: 10.1039/x0xx00000x

Mattia Lopresti[a], Łukasz Kurowski[b], Luca Palin[a], Marco Milanesio[a*], Magdalena Siedzielnik[b], Karolina Gutmańska[b], Adriana Dobrenko[b], Tomasz Klimczuk[c], Ewelina Pawelczyk[b,d], Anna Dołęga[b$]

Nanocrystalline powders of monometallic and bimetallic imidazolates of Co, Zn and Ag were produced by a reaction carried out in water. The powders were characterized by powder X-ray diffraction and the crystal structures of new compounds $Ag_2ZnIm_4$ and $Ag_2CoIm_4$ (Im = imidazolate) were solved. Heterometallic Co/Zn imidazolates showed the standard ZIF-8 crystal structure while Ag/Zn and Ag/Co systems were isostructural with the copper analogs. The powders were further characterized by EDX, UV-Vis and FTIR ATR spectroscopy in solid state. The catalytic experiments indicated that out of the studied heterometallic compounds only $Ag_2Co(Im)_4$, exhibits some catalytic activity in the reaction of oxidation of 1-phenylethanol by *tert*-butylhydroperoxide at elevated temperature.

## Introduction

ZIFs (zeolitic imidazolate frameworks) are a class of MOFs with the porous, zeolite-like structures. Being metal imidazolates, $M(Im)_2$ (M = Zn, Co, Cu, Fe, other, Im = 1,3-$N_2C_3H_3$), the structure of the prototypical compound ZIF-8, formally with chemical formula $Zn(Im)_2$, is built by $Zn(Im)_4$ tetrahedra. The two M-N bonds at one imidazolate ligand are oriented at an angle of about 144°, close to the Si-O-Si angle in quartz or porous zeolites (Figure 1).[1-3] Some of these compounds exhibit structural flexibility and transform under pressure,[4-7] as a result of gas adsorption or the change in the temperature.[7-9] The structural changes result from the rotations of the imidazolate and may lead from porous to dense phases.[9] The structural similarity to 3-D network of silicates results in the unique glass-forming capability of ZIFs.[10-14] It is possible to quench the melted ZIFs to obtain inorganic-organic glasses with interesting physical properties such as ionic conductivity[11,14] or selective sorption of hydrocarbons.[12] The mechanism of glass formation includes rapid de-/re-coordination of imidazolate linkers, which is true for diverse ZIF topologies.[10]

Both open framework structures and relatively dense metal imidazolates may have potential industrial utility especially considering their excellent thermal properties.[2,15-17] ZIFs are candidates for selective membrane materials in the process of $CO_2$ capture and purification of petrochemical gas,[18-20] catalysis,[16] electrocatalysis,[17] lithium storage,[21] luminescent materials and detectors,[22-24] magnetic materials,[25] removal of heavy metals from the wastewater.[26] As previously mentioned, ZIFs can work as materials reversibly responsive to the changes of the external environment and this property can be tuned e.g. by the volume of the imidazolate linker.[27]

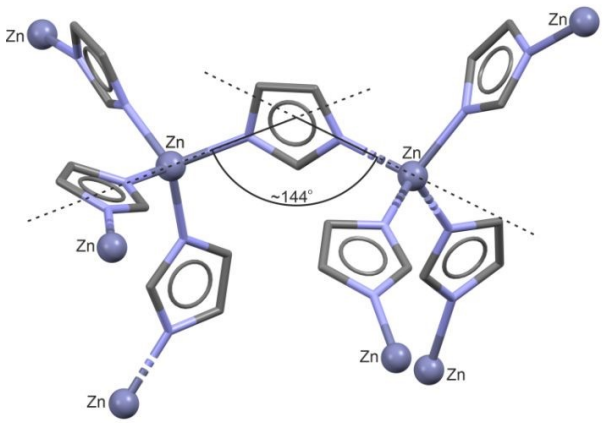


**Figure 1.** The molecular structure of ZIF-8.[3]

The synthesis of imidazolates is relatively simple and requires mixing the solution of imidazole with the solution of metal salt with or without heating.[26,28-32] However, the change in the pH typically with ammonia,[28,33] or sodium hydroxide,[34] may lead to the formation of different polymorphs. In the case of a simple Cu(II) imidazolate of $Cu(Im)_2$ stoichiometry, five different

[a] aDipartimento di Scienze e Innovazione Tecnologica and CrisDi Interdepartmental Center for Crystallography, Università del Piemonte Orientale Viale T. Michel 11, 15121 Alessandria, Italy.
[b] Department of Inorganic Chemistry, Chemical Faculty, Gdansk University of Technology, Narutowicza St. 11/12, 80-233, Gdańsk, Poland
[c] Faculty of Applied Physics and Mathematics and Advanced Materials Centre, Gdansk University of Technology, Narutowicza St. 11/12, 80-233, Gdańsk, Poland.
[d] Department of Process Engineering and Chemical Technology, Chemical Faculty, Gdansk University of Technology, Narutowicza St. 11/12, 80-233, Gdańsk, Poland
* E-mail: marco.milanesio@uniupo.it
$ E-mail: anna.dolega@pg.edu.pl
Electronic Supplementary Information (ESI) available: [Bond lengths and the discussion of crystal packing, FTIR ATR Spectra, Band gaps, TG/DTG diagrams, yields of catalysed reactions]. See DOI: 10.1039/x0xx00000x

View Article Online
DOI: 10.1039/D3DT03211F



networks (polymorphs) were isolated and structurally characterized in this way.[35,36] Various structure-directing agents Bond lengths,amines,[37,38] bulky amides,[39] or cetyltrimethylammonium bromide (CTAB).[17] Though the synthesis of imidazolates is usually carried out in the basic pH, they are also able to crystallize from acidic solutions. The syntheses in diluted acid solutions were described as acid-catalyzed, which referred to the dissolution of basic metal precursor such as metal oxide in the diluted, aqueous solution of the acid.[15,40] Variations of the solution methods include solvothermal synthesis in different solvents,[19,25,41,42] ionothermal method in deep eutectic solvents (DES),[43] or ionic liquids (ILs).[44] From the reactive metal precursors such as alkaline earth metals, their hydrides, or borohydrides, the imidazolates can be obtained in solvent-free reactions: *via* mechanosynthesis,[45] or *via* the direct reaction of the metal or metal hydride with imidazole in the melt (melt synthesis).[22,23,46-48] Less reactive precursors require liquid assisted grinding (LAG), as described for the fast synthesis of ZIF-4 from ZnO and imidazole,[49] and other mixed-metal and mixed ligand networks.[50] The LAG syntheses were carried out in the presence of dimethylformamide (DMF) and catalytic amounts of inorganic salts e.g. metal acetates.[50] Template-assisted mechanochemical synthesis with the further vapor aging (DMF or DEF) was also reported.[51]

The structure and properties of ZIF materials can be modified by the substitution of metal ions and/or ligands within the primary network. Apart from simple monometallic systems, some heterometallic imidazolates were reported. These include solid solutions in which the metal ions may substitute one another in practically any ratio or heterometallic compounds with the defined composition. The Co(II)/Zn(II) ZIFs,[20,26] or $[Sr_{1-x}Eu_x(Im)_2]_\infty$,[52] are examples of the solid solutions. The pairs of cations Co(II)/Zn(II) and Sr(II)/Eu(II) have very similar ionic radii and they form isomorphic compounds. The examples of heterometallic compounds include $Cu_2Co(Im)_4$,[53] $Cu_2Zn(Im)_4$,[15] and other Cu/Zn systems described later,[18] alkali and alkaline earth metals imidazolates $NaMgIm_3$ and $KMgIm_3$.[45] Variable oxidation numbers of the same element may also lead to the new topology of the network as in mixed-valence Cu(I)/Cu(II),[54,55] or Co(II)/Co(III) imidazolates.[17] Apart from simple imidazole, the alkyl-substituted imidazole derivatives,[56] as well as benzimidazoles/alkyl-substituted benzimidazoles,[27,42,57] or amino(benz)imidazoles,[19] are applied in the synthesis of ZIF materials. In certain conditions imidazolate/imidazol (neutral molecule) complexes can be isolated.[24,46-48,58,59] Heteroligand e.g. imidazole/benzimidazole systems were described.[11-14,19,21,42]

The substitution of ligand and metal ion – even with non-metals - is also possible as in a series of metal carboxylate boron imidazolate frameworks.[60]

In order to modify their useful properties ZIFs were also applied as constituents of composite materials. Pure ZIF-8, which has a wide band gap of 4.9 eV, was not only doped with other metal ions but also combined with the metal oxides to form a core–shell/composite of enhanced photocatalytic activity. The bandgap of the composite was reduced to less than 2.0 eV and the material was successfully used in the photocatalytic desulphurization of model fuels.[56]

In this study, we introduce a simple wet reaction method, highlighting the utilization of water as a solvent for the efficient synthesis of metal imidazolate materials. In this way we initially produced known solid solutions $Zn_xCo_{1-x}(Im)_2$, and then new heterometallic compounds: $Ag_2Co(Im)_4$ and $Ag_2Zn(Im)_4$. We utilized higher zinc and lower cobalt concentrations throughout the synthesis of Zn/Co systems. This choice was driven by the fact that the price of cobalt is approximately 15 times higher than that of zinc. Our objective was to assess the stability of heterometallic imidazolates while minimizing the content of cobalt(II). For the obtained compounds, we report their crystal structures, X-ray powder diffraction, FTIR, SEM-EDX and UV-Vis spectroscopic results as well as the results of catalytic studies for the oxidation of 1-phenylethanol.

## Experimental

### Syntheses

Substrates: imidazole, $Co(NO_3)_2{\cdot}6H_2O$, $Zn(NO_3)_2{\cdot}6H_2O$, $AgNO_3$, sodium hydroxide (Merck) and 25% ammonium in water (POCh, Poland) were purchased from commercial sources.

Compounds **1** (cobalt(II) imidazolate, $Co(Im)_2$), **2** (zinc(II) imidazolate, $Zn(Im)_2$), **3** (silver imidazolate, AgIm), **4a**, **4b**, **4c**, **4d**, **4e**, (Co(II)/Zn(II) imidazolates) **5** (Zn(II)/Ag(I) imidazolate) and **6** (Co(II)/Ag(I) imidazolate) were obtained according to the simple general procedure involving mixing of an aqueous 1 M solution of imidazole with the aqueous solution of a base: 1 M sodium hydroxide or concentrated 25% ammonia and subsequent addition to an aqueous solution containing one or two metal nitrates. The final reaction mixture was stirred for 15-30 minutes at RT, which, in some cases, allowed to reach almost 100% yield; solid residue was separated by centrifugation and decantation. The precipitate was washed three times by 30 ml of distilled water, which was each time removed by centrifugation and decantation (20 min/ 5000 rpm/20 °C). The obtained samples were dried in a laboratory drier at 80°C, for 24 h. The amounts, final concentrations of the reacting solutions and yields are given in Tables 1 and 2. The final purities of the obtained products were evaluated on the basis of elemental analyses and FTIR spectra, which showed the absence or presence of the imidazole impurity. The data are collected in Table 3. We have never observed the presence of inorganic salts (nitrates) either in the FTIR spectra or X-ray powder diffraction (XRPD) pattern. The Rietveld refinement of powder diffraction patterns, with absence of extraphases, confirmed a purity larger than 99%.

## ARTICLE

**Table 1**. Optimization of the synthesis of **1,** and the results of the syntheses of **2** and **3** in the presence of sodium hydroxide.

| Compd. number | Vol. of **0.05M** $M(NO_3)_2$ or $AgNO_3$ [$cm^3$] | Conc. of $M^{2+}$ or $Ag^+$ in the final solution [$mol/dm^3$] | Vol. of **1M** solution of imidazole [$cm^3$] | Concentration of imidazole in the final solution [$mol/dm^3$] | **Molar ratio $M^{2+}$ or $Ag^+$ : imidazole** | Vol. of **1M** solution of NaOH [$cm^3$] | Concentration of NaOH in the final solution [$mol/dm^3$] | Vol. of water [$cm^3$] | Final vol. [$cm^3$] | Mass of the product [mg] | Yield [%] (comments) |
|---|---|---|---|---|---|---|---|---|---|---|---|
| **1** | 10 | 0.0167 | 10 | 0.33 | **1 : 20** | 0 | | 10 | 30 | 6.8 | 7.12 |
| | 10 | 0.0167 | 10 | 0.33 | **1 : 20** | 0.5 | 0.0167 | 9.5 | 30 | 44.1 | 46.2 |
| | 10 | 0.0167 | 10 | 0.33 | **1 : 20** | 1.0 | 0.033 | 9.0 | 30 | 98.0 | 102.6 |
| | 10 | 0.0167 | 10 | 0.33 | **1 : 20** | 2.5 | 0.083 | 7.5 | 30 | 97.4 | 101.6 |
| | 10 | 0.0167 | 10 | 0.33 | **1 : 20** | 5.0 | 0.167 | 5 | 30 | 112.0 | 117.3 (contains imidazole impurity) |
| | 10 | 0.0167 | 10 | 0.33 | **1 : 20** | 7.5 | 0.25 | 2.5 | 30 | 100.0 | 104.7 (contains imidazole impurity) |
| | 10 | 0.0167 | 5.0 | 0.165 | **1 : 10** | 1.0 | 0.033 | 14 | 30 | 76.7 | 79.5 |
| | 10 | 0.0167 | 2.0 | 0.067 | **1 : 4** | 1.0 | 0.033 | 17 | 30 | 72.7 | 75.3 |
| | 10 | 0.0167 | 1.0 | 0.033 | **1 : 2** | 1.0 | 0.033 | 18 | 30 | 55.7 | 57.7 |
| **2** | 10 | 0.0167 | 5.0 | 0.165 | **1 : 10** | 1.0 | 0.033 | 14 | 30 | 48.4 | 48.6 |
| **3** | 10 | 0.0167 | 5.0 | 0.165 | **1 : 10** | 1.0 | 0.033 | 14 | 30 | 40.6 | 46.4 |

ARTICLE

**Table 2.** The results of the syntheses of **1** - **6** in the presence of ammonia.

| Homometallic imidazolates* | | | | | | | | | | | |
|---|---|---|---|---|---|---|---|---|---|---|---|
| Compd. number | Vol. **0.05**M $M(NO_3)_2$ or $AgNO_3$ [$cm^3$] | Conc. of $M^{2+}$ or $Ag^+$ in the final solution [$mol/dm^3$] | - | - | - | Vol. **1M** imidazole [$cm^3$] | Vol. **25%** $NH_3$ [$cm^3$] | Vol. of water [$cm^3$] | Final vol. [$cm^3$] | Mass of the product [mg] | Yield [%] |
| 1 | 10 | 0.0167 | - | - | - | 5.0 | 0.5 | 14.5 | 30 | 86.0 | 89.1 |
| 2 | 10 | 0.0167 | - | - | - | 5.0 | 0.5 | 14.5 | 30 | 74.6 | 75.0 |
| 3 | 10 | 0.0167 | - | - | - | 5.0 | 0.5 | 14.5 | 30 | 66.3 | 75.8 |
| Co,Zn heterometallic imidazolates* | | | | | | | | | | | |
| Compd. number | Vol. 0.05M $Co(NO_3)_2$ [$cm^3$] | Conc. of $Co^{2+}$ in the final solution [$mol/dm^3$] | Vol. 0.05M $Zn(NO_3)_2$ [$cm^3$] | Conc. of $Zn^{2+}$ in the final solution [$mol/dm^3$] | Molar ratio $Co^{2+}$ : $Zn^{2+}$ in the final solution | Vol. 1M imidazole [$cm^3$] | Vol. 25% $NH_3$ [$cm^3$] | Vol. of water [$cm^3$] | Final vol. [$cm^3$] | Mass of the product [mg] | Yield [%] |
| 4a | 1 | 0.00167 | 9 | 0.015 | 1 : 9 | 5.0 | 0.5 | 14.5 | 30 | 40.1 | 38.5 |
| | 5 | 0.00167 | 45 | 0.015 | 1 : 9 | 25.0 | 2.5 | 72.5 | 150 | 423.5 | 81.3 |
| | 5 | 0.00167 | 45 | 0.015 | 1 : 9 | 25.0 | 2.5 | 72.5 | 150 | 311.0 | 60.1 |
| 4b | 4.15 | 0.0014 | 45.85 | 0.0153 | 1 : 11 | 25.0 | 2.5 | 72.5 | 150 | 401.2 | 79.9 |
| 4c | 3.33 | 0.0011 | 46.67 | 0.0155 | 1 : 14 | 25.0 | 2.5 | 72.5 | 150 | 377.7 | 75.6 |
| | 3.33 | 0.0011 | 46.67 | 0.0155 | 1 : 14 | 25.0 | 2.5 | 72.5 | 150 | 346.0 | 66.9 |
| 4d | 2.8 | 0.00093 | 47.2 | 0.0157 | 1 : 17 | 25.0 | 2.5 | 72.5 | 150 | 407.3 | 81.4 |
| 4e | 0.5 | 0.00083 | 9.5 | 0.016 | 1 : 19 | 5.0 | 0.5 | 14.5 | 30 | 39.8 | 39.3 |
| | 2.5 | 0.00083 | 47.5 | 0.016 | 1 : 19 | 25.0 | 2.5 | 72.5 | 150 | 422.6 | 83.4 |

*concentration of imidazole 0.165 $mol/dm^3$ and concentration of ammonia 0.222 $mol/dm^3$in all experiments.

**Table 2 ctd.** The results of the syntheses of **1** - **6** in the presence of ammonia.

| Ag,Zn and Ag,Co heterometallic imidazolates* | | | | | | | | | | | |
|---|---|---|---|---|---|---|---|---|---|---|---|
| | Vol. 0.05M $AgNO_3$ [$cm^3$]/ [$mol/dm^3$] | Conc. of $Ag^+$ in the final solution [$mol/dm^3$] | Vol. 0.05M $Zn(NO_3)_2$ [$cm^3$]/ | Conc. of $Zn^{2+}$ in the final solution [$mol/dm^3$] | Molar ratio $Ag^+ : Zn^{2+}$ in the final solution | Vol. 1M imidazole [$cm^3$] | Vol. 25% $NH_3$ [$cm^3$] | Vol. of water [$cm^3$] | Final vol. [$cm^3$] | Mass of the product [mg] | Yield [%] comments |
| 5 | 3.3 | 0.0055 | 6.7 | 0.011 | 1 : 2 | 5.0 | 0.5 | 14.5 | 30 | 41.0 | 89.9 per Ag |
| | 7.5 | 0.0125 | 2.5 | 0.0042 | 2.4 : 1 | 5.0 | 0.5 | 14.5 | 30 | 60.4 | 87.4 per Zn |
| | 33 | 0.011 | 17 | 0.0057 | 2 : 1 | 25.0 | 2.5 | 72.5 | 150 | 253.0 | 55.8 per Zn and Ag |
| | Vol. 0.05M $AgNO_3$ [$cm^3$]/ | Conc. of $Ag^+$ in the final solution [$mol/dm^3$] | Vol. 0.05M $Co(NO_3)_2$ [$cm^3$]/ | Conc. of $Co^{2+}$ in the final solution [$mol/dm^3$] | Molar ratio $Ag^+ : Co^{2+}$ in the final solution | Vol. 1M imidazole [$cm^3$] | Vol. 25% $NH_3$ [$cm^3$] | Vol. of water [$cm^3$] | Final volume [$cm^3$] | Mass of the product [mg] | Yield [%] comments |
| 6 | 13.2 | 0.0048 | 26.8 | 0.0097 | 1 : 2 | 25.0 | 2.5 | 70 | 137.5 | 139.9 | 77.4 per Ag |
| | 33 | 0.011 | 17 | 0.0057 | 2 : 1 | 25.0 | 2.5 | 72.5 | 150 | 391.0 | 72.0 per Ag and Co |

*concentration of imidazole 0.165 $mol/dm^3$ and concentration of ammonia 0.222 $mol/dm^3$in all experiments.

**Table 3** The elemental analysis and FTIR data for **1** - **6**.

| | Assumed formula | Elemental analysis calculated [%] | | | Elemental analysis experimental [%] | | | FTIR [$cm^{-1}$] |
|---|---|---|---|---|---|---|---|---|
| | | C | N | H | C | N | H | |
| **1** | $CoC_6N_4H_6$ | 37.32 | 29.02 | 3.13 | 36.75 | 28.09 | 4.04 | 3109(vw), 1658(vw), 1596(w), 1488(s), 1466(s), 1315(m), 1277(w), 1233(m), 1164(m), 1105(w,sh), 1079(vs), 978(w), 952(s), 828(m), 771(w,sh), 751(s), 664(s) |
| **2** | $ZnC_6N_4H_6$ | 36.12 | 28.08 | 3.03 | 35.59 | 27.83 | 3.96 | 3109(vw), 1666(vw), 1601(w), 1495(s), 1472(m), 1320(m), 1283(w), 1238(m), 1169(m), 1106(w,sh), 1084(vs), 979(w), 952(s), 832(m), 774(m,sh), 755(s), 666(s), 649(vw,sh) |
| **3** | $AgC_3N_2H_3$ | 20.60 | 16.01 | 1.73 | 20.47 | 16.03 | 2.165 | 3126(m), 3112(m), 2579(vw), 2509(vw), 1671(w), 1645(vw), 1568(m), 1487(m,sh), 1478(m,sh), 1462(s), 1301(vw), 1281(m), 1236(m), 1172(m), 1108(m,sh), 1088(s), 969(w), 946(m), 849(m), 839(m), 776(w,sh), 759(m,sh), 749(m,sh) 739(vs), 664(s) |
| **4a** | $CoZn_9(C_6N_4H_6)_{10}$* | 36.24 | 28.17 | 3.04 | 36.20 | 28.14 | 4.10 | 3109(vw), 2771(vw), 2598(vw), 2516(vw), 2485(vw), 1665(w), 1600(w), 1494(s), 1471(m), 1320(m), 1282(w), 1238(m), 1169(m), 1106(w,sh), 1083(vs), 979(vw), 952(s), 832(m), 774(m,sh), 755(s), 666(s), 648(vw,sh) |
| **4b** | $CoZn_{11}(C_6N_4H_6)_{12}$* | 36.22 | 28.16 | 3.04 | 36.11 | 28.09 | 4.01 | |
| **4c** | $CoZn_{14}(C_6N_4H_6)_{15}$* | 36.20 | 28.14 | 3.04 | 35.93 | 27.96 | 4.00 | |
| **4d** | $CoZn_{17}(C_6N_4H_6)_{18}$* | 36.18 | 28.13 | 3.04 | 37.23 | 28.43 | 3.03 | |
| **4e** | $CoZn_{19}(C_6N_4H_6)_{20}$* | 36.18 | 28.13 | 3.04 | 35.52 | 27.64 | 3.99 | |
| **5** | $Ag_2ZnC_{12}N_8H_{12}$ | 26.23 | 20.40 | 2.20 | 26.16 | 20.43 | 2.92 | 3133(w), 3110(w), 2589(vw) 2510(vw), 2324(vw), 1698(vw), 1680(vw), 1653(vw), 1617(w), 1544(vw), 1488(s), 1464(s), 1317(w), 1277(w), 1239(m), 1170(m), 1110(w,sh), 1085(vs), 977(vw), 951(s), 828(s), 768(s), 663(vs), 644(w,sh) |
| **6** | $Ag_2CoC_{12}N_8H_{12}$ | 26.55 | 20.64 | 2.23 | 26.39 | 21.16 | 2.83 | 3132(w), 3118(w), 2583(vw) 2504(vw), 1695(vw), 1650(w), 1615(w), 1481(s), 1461(s), 1314(m), 1273(w), 1237(m), 1167(m), 1110(m,sh), 1084(vs), 976(vw), 952(m), 825(s), 767(s), 662(s), 642(w,sh) |

*The calculated analysis is given for the molar ratio of cobalt(II) and zinc(II) in the initial solution but the composition of the solid is not necessarily the same and it served to calculate the experimental ratio. Sample 4d was probably contaminated or there was a mistake in the sample preparation by the operator.

View Article Online
DOI: 10.1039/D3DT03211F

ARTICLE





### Catalytic study

The potential catalytic properties of complexes: **4e**, **5** and **6** was investigated in a redox reaction between the *tert*-butylhydroxyperoxide (Luperox TBH70X) and 1-phenylethanol, leading to the formation of acetophenone. Variable temperature experiments up to 80 °C were performed; *tert*-butylhydroxyperoxide starts to decompose at its boiling point of 89 °C/760 mmHg.[61] The quantities of the substrate (1-phenylethanol) and product (acetophenone) were determined by gas chromatography (GC) using the internal standard method. Benzaldehyde was used as internal standard. We used the Thermo Finningan Focus gas chromatograph with the Thermo Scientific TRACE TR-5MS GC capillary column (30 m). The Chrom Card software was used to analyse the data. Please refer to Mielcarek et al. (2019) for further details of the experiment.[62]

Samples for the experiments were prepared by mixing 1-phenylethanol (0.605 ml, 5 mmol) with Luperox TBH70X (70 wt%; 1.384 ml, 10 mmol). Two independent test tubes were prepared: one with the addition of selected complex (**4e**, **5** and **6**, 0.0145 g/0.0290 g) as a catalyst and the other without catalyst. The test was carried out on both samples simultaneously.

### Physical measurements

### Structure solution by X-ray Powder Diffraction

ZIF samples **1**, **4a-e**, **5** and **6** underwent characterization using a Bruker D8 Advance diffractometer, equipped with a copper K$\alpha$ X-ray source and a LynxEye XE-T detector. The measurement conditions involved a current of 40 mA and an electric potential of 40 kV for the source. The goniometer's radius was set at 280 mm under standard measurement conditions. The experimental data are collected in Table 4.

**Table 4**. XRPD experimental data for **1**, **4c**, **5** and **6**.

| Compound | **1** | **4c** | **5** | **6** |
|---|---|---|---|---|
| Chemical formula | $C_6H_6CoN_4$ | $C_{12}H_{12}Co_{0.13}N_8Zn_{1.87}$ | $C_{12}H_{12}Ag_2N_8Zn$ | $C_{12}H_{12}Ag_2N_8Co$ |
| Formula weight/g·mol$^{-1}$ | 398.20 | 398.20 | 549.43 | 542.97 |
| Crystal system | Tetragonal | Tetragonal | Tetragonal | Tetragonal |
| Space group | $I4_1cd$ (110) | $I4_1cd$ (110) | $P\text{-}42_1c$ (114) | $P\text{-}42_1c$ (114) |
| a/Å | 23.552(3) | 23.5344(1) | 11.3668(3) | 11.3300(4) |
| b/Å | 23.552(3) | 23.5344(1) | 11. 3668(3) | 11.3300(4) |
| c/Å | 12.473(3) | 12.4751(6) | 6.27238(4) | 6.2085(2) |
| $\alpha$/° | 90 | 90 | 90 | 90 |
| β/° | 90 | 90 | 90 | 90 |
| γ/° | 90 | 90 | 90 | 90 |
| V/Å$^3$ | 6918(3) | 6909.3(3) | 810.42(4) | 796.98(6) |
| Z | - | 16 | 2 | 2 |
| T/K | 298 | 298 | 298 | 298 |
| $l_{Cu\ Ka}$/Å | 1.54175 | 1.54175 | 1.54175 | 1.54175 |
| $r_{calc}$/g·cm$^{-3}$ | - | 1.531 | 2.252 | 2.263 |
| F000 | - | 3193.5 | 528.0 | 522.0 |
| F000’ | - | 3148.51 | 526.56 | 519.19 |
| m/mm$^{-1}$ | - | 4.259 | 21.016 | 27.672 |
| $R_p$ | - | 4.941 | 7.704 | 1.986 |
| $R_{wp}$ | - | 7.793 | 10.935 | 3.070 |
| CCDC number | - | 2285711 | 2285708 | 2285710 |

For **1** the data were collected from 2θ = 5° to 40°, with the 0.01° step. The profile fitting (LeBail refinement) of the XRPD pattern was performed to determine the crystal structure type and lattice parameters of the two tested samples of **1**, using HighScore Plus ver. 3.0e software.

View Article Online DOI: 10.1039/D2DT03215



The XRPD measurement of the ZIF samples **4e** – **6** were performed with two different methods, depending on the amount of the samples: for samples available in small amounts, capillary measurements were performed in Debye-Scherrer geometry while, for more abundant samples, standard Bragg-Brentano geometry setup with variable slits was exploited. When using the capillary stage primary optics included Göbel mirrors with a 1 mm focusing hole and planar 0.6 mm slits. Soller slits were mounted on both the primary and secondary optics. The ZIF samples were contained in a 0.7 mm glass capillary. The measurements were conducted for approximately 6 hours, covering a range of $2\theta$ from 2 to 70 degrees with a step size of 0.015 degrees per step and an irradiation time of 5 seconds per step. Bragg-Brentano geometry was carried out employing variable width slits as primary optics to maintain a constant portion of the irradiated sample at 17 mm. Soller slits with a 2.5-degree angle were used on both primary and secondary optics to minimize the impact of axial divergence. Patterns were collected in an angular range of 2 to 130 degrees in $2\theta$, with a step size of 0.02 degrees per step and a collection time of 4 seconds per step. Before attempting indexation and crystal structure solution, existing literature on crystal structures was thoroughly reviewed to exclude any homology with previously published structures. For the new structures, indexing was performed using EXPO2014 and Topas 7. The structure solution involved the parallel usage of Topas and EXPO, employing the simulated annealing method in direct space to explore at best all the possible solution. The three crystal structures, representative of all analyzed samples, have been submitted to CCDC with deposition numbers 2285708 (Compound **5**), 2285710 (Compound **6**), 2285711 (Compound **4**).

**UV-Vis diffuse reflectance spectroscopy in solid state**

The solid state diffuse reflectance spectra were carried out using the Perkin Elmer Lambda 365+ double-beam UV/Vis spectrometer with an integrating sphere. Barium Sulphate ($BaSO_4$) was used as a blank reference for the reflectance spectra in the range of 200 – 1100 nm with a slit width of 5 nm and scan speed 489 nm/min. The Kubelka-Munk transformation was applied to the reflectance data for estimation of the energy band gap ($E_g$).[63] Data evaluation was performed with the UV WinLab Data Processor and Viewer Version 10.6.2 software tool. Sample preparation consisted of mixing and grinding 10 mg of the test compound with 450 mg of $BaSO_4$. UV-Vis spectra of the complexes in the solid state were analyzed and compared with the spectra of simple metal-imidazole compounds (**1**-**3**).

**FTIR ATR spectroscopy**

FTIR was recorded with Nicolet iS50 equipped with Specac **Q**uest diamond ATR device. All spectra were collected and formatted by OMNIC software.

**SE microscopy (SEM) and EDX spectroscopy**

The morphology and composition of the samples were examined with a scanning electron microscope (FEI Quanta 250 FEG) equipped with an energy-dispersive X-ray (EDX) spectrometer.

**TG analysis**

Thermal stability of compounds **4a**, **4c**, **5** and **6** was examined using thermogravimetric analysis. TG/DTG patterns were measured and recorded by a METTLER TOLEDO thermogravimetric analyzer. The samples were heated from 25 to 1100 °C (heating rate 10 °C/min) in air flow of 40 ml/min.

## Results and Discussion

**Syntheses**

Metal imidazolates are coordination polymers (CPs) in which the imidazolate anion serves as bridging unit and, as such, they are insoluble in most solvents, at least if the solvent does not change the structure of the CP by coordination. Therefore, it is possible to precipitate metal imidazolates from the aqueous solutions, in which both precursors: selected metal salts and imidazole are well-soluble. We have carried out the syntheses in such a way that we prepared *in situ* imidazolate salts by mixing imidazole solutions with the solution of a base: sodium hydroxide or ammonia and subsequently added the as-prepared solution of imidazolate to the solution of metal nitrate. The combination of these two solutions results in the immediate precipitation of the corresponding metal imidazolate in the form of a nanocrystalline powder. We have optimized the concentrations of deprotonating agent (NaOH) and imidazole with regard to the final yield of metal imidazolate for the synthesis of cobalt(II) imidazolate **1** (Table 1). It is possible to achieve a 100% yield in this system. However, using a large excess of imidazole to enhance product yield results in contamination of the precipitate with imidazole, making it challenging to remove the compound through repeated washings (refer to FTIR spectroscopy results). While sodium hydroxide serves as an effective deprotonating agent in the synthesis of cobalt(II) imidazolate **1**, we had to substitute it with ammonia for the syntheses of zinc and silver imidazolates due to very poor yields in the presence of sodium hydroxide (not shown in Table 1). We believe that the low yields of silver- and zinc-containing imidazolates in the presence of sodium hydroxide are attributed to additional equilibrium reactions occurring between silver(I)/zinc(II) ions and sodium hydroxide or sodium imidazolate in water. In the case of silver(I), it leads to the precipitation of $Ag_2O$, while zinc(II) forms water-soluble hydroxocomplexes due to its amphoterism. We did not reach that high, 100% yields of imidazolate formation in the presence of ammonia (Table 2). A likely explanation is the formation of water-soluble complexes with ammonia by the metal ions. Indeed, this is a competitive reaction observed across all studied metal ions: Ag(I), Co(II), and Zn(II). Below is a non-exhaustive list of the possible simple reactions occurring in the studied systems:

$$ImH + NaOH = ImNa + H_2O$$
$$ImH + NH_3 = ImNH_4$$
$$Co(NO_3)_2 + 2ImNa = Co(Im)_2\downarrow + 2NaNO_3$$
$$Co(NO_3)_2 + 2ImNH_4 = Co(Im)_2\downarrow + 2NH_4NO_3$$
$$Zn(NO_3)_2 + 2ImNH_4 = Zn(Im)_2\downarrow + 2NH_4NO_3$$
$$AgNO_3 + ImNH_4 = AgIm\downarrow + NH_4NO_3$$

$$Zn(NO_3)_2 + 4NaOH = Na_2[Zn(OH)_4] + 2NaNO_3$$
$$2AgNO_3 + 2NaOH = Ag_2O\downarrow + 2NaNO_3 + H_2O$$
$$Co(NO_3)_2 + 4NH_3 = [Co(NH_3)_4](NO_3)_2$$
$$Zn(NO_3)_2 + 4NH_3 = [Zn(NH_3)_4](NO_3)_2$$
$$AgNO_3 + 2NH_3 = [Ag(NH_3)_2]NO_3 \text{ etc.}$$

Due to the formation of several water-soluble by-products, such as simple salts and metal complexes, the residue requires careful washing with water.

Apart from homometallic systems, we have also tested metal mixtures and thus we confirmed that zinc and cobalt imidazolates form solid solutions with variable metals ratios. However, in the case of cobalt-silver and zinc-silver mixtures, the obtained precipitates have a defined stoichiometry. Thus, the latter are new chemical compounds, which we further characterized by X-ray diffraction, by solving and refining their crystal structures. The UV-Vis, powder diffraction and other data that confirm such conclusions will be described in the following sections. Moreover, the elemental analysis data, which are collected in Table 3 reasonably correspond to the assumed composition of the compounds **1**-**6**, with the larger deviation only for the sample of **4d**. Interestingly, heterometallic Ag/Co imidazolates were attempted by Tian and coworkers with the conclusion that under solvothermal conditions, a metal imidazolate complex containing Ag(I) cannot be obtained due to the highly oxidative nature of Ag(I).[53] Moreover, the compounds were later mentioned by Zhang and Chen (2006) but finally, at least to our knowledge, never reported.[55]

We conducted the reactions on two different scales and observed that increasing the scale generally had a significantly positive impact on the reaction yield. A five-fold increase in the reaction volume (with no change in the concentrations of the reactants) resulted in a two-fold increase in the yield (see Table 2). This is likely attributed to a lower percentage of product loss during its recovery from the post-reaction mixture.

It should be observed that metal imidazolates are metal complexes and though they do not dissolve in neutral and basic solutions, they are unstable in the presence of acids, which protonate the imidazolate ligand. We have observed immediate dissolution of the precipitates even in the presence of diluted acetic acid.

Finally we would like to mention that in the carefully outgassed water it is possible to obtain blue-green iron(II) imidazolate in the same way as cobalt(II) imidazolate. The obtained powder undergoes immediate oxidation in the presence of air, which is manifested by the change of colour from green to brown and we did not study it further.

**XRPD, SEM, EDX data, crystal structures**

Bimetallic compounds based on Co, Zn and Ag atoms and imidazole as organic counterpart were prepared by the green synthesis approach described in the experimental section, also varying the metal ration to assess the effect of the starting composition on the purity and crystallinity of the obtained products. Their crystallinity and purity were assessed by powder diffraction. Figure 2 presents XRPD pattern for cobalt(II) imidazolate **1**. The experimental data are represented by blue dots, a red solid line is the profile fit (LeBail) and the vertical bars show the expected Bragg reflections for the used model. As a result of the synthesis in water the compound crystallized in a tetragonal *I*41*cd* (110) space group with the refined lattice parameters a = 23.552(3) Å and c = 12.473(3) Å. The averaged crystallite size d = 80 nm was roughly estimated using the Scherrer equation based on the corrected full width at half maximum (FWHM) of the (402) XRD reflection. The broad hump (background) at low 2θ angle is likely caused by substantial fraction of the amorphous phase. Both tested samples from two synthetic attempts returned the same XRPD pattern.

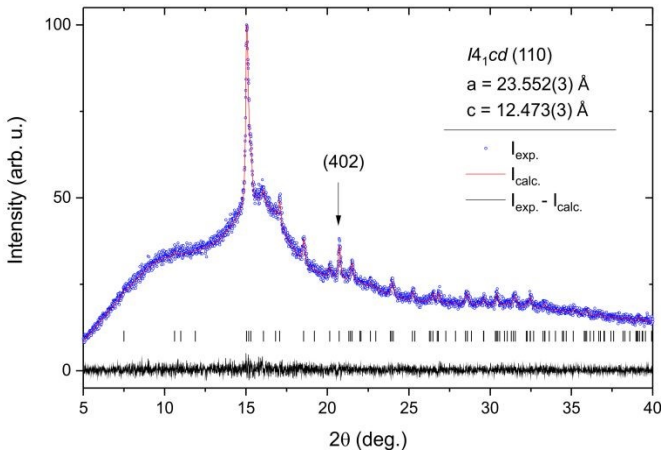


**Figure 2.** XRPD patterns for compound **1** of the general formula $CoIm_2$.

The heterometallic compounds can be categorized within two categories, the first one comprising **4a-e** and the second one **5** and **6**. Compounds collectively denoted as **4a – 4e** have $Co_xZn_{(1-x)}Im_2$ formula, where 0<x<1. They are all isostructural with the Zn-*zni* phase first reported by Lehrnert & Seel in 1980, which means that similar to **1** they have tetragonal unit cell, space group $I4_1cd$ with the cell parameters: a=b=23.5331(15), c=12.4723(13), V=6907.3(11) measured at RT (Figure 3).[25,64,65] The **4c** data correspond to the best set of data in Figure 3 and were thus used for the Rietveld refinement (Figure 4) against literature data, since it is isostructural to CCDC 1180194.[25,36,64]

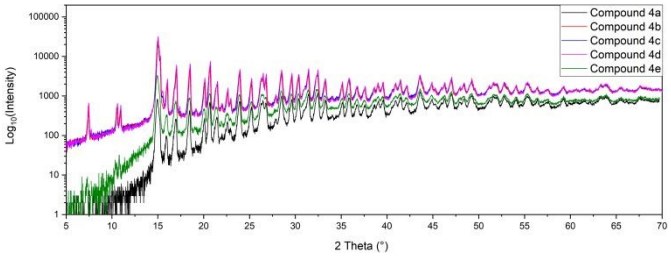


**Figure 3.** XRPD patterns for compounds 4a-4e of the general formula $Co_xZn_{(1-x)}Im_2$, where 0<x<1.

View Article Online
DOI: 10.1039/D3DT03415

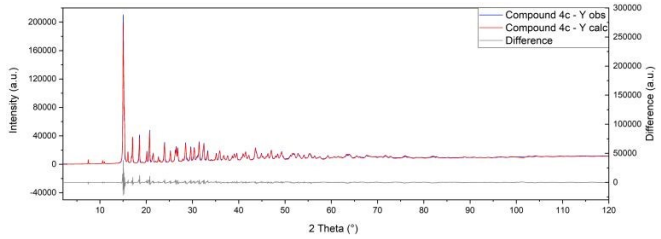


**Figure 4.** The results of the Rietveld refinement of **4c.**

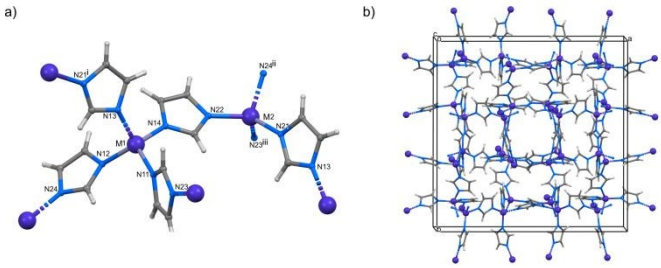


**Figure 5**. The molecular structure of **4c**, M=Zn or Co: a) independent unit with an additional imidazole ring to illustrate the tetrahedral environment of the metal ion; b) crystal packing viewed along axis *c*. Bond lengths range: M-N 1.981-2.007 Å; Angles range N-M-N 103.44-116.44°; symmetry operations: [i] –x, ½-y, ¼+z; [ii] 1/2–x, y, -3/4+z; [iii] ½+x, y, -1/4+z.

The obtained crystal structure is illustrated in Figure 5. In Figure 5a we show slightly more than independent unit with the two crystallographically unique Co/Zn atoms and in Figure 5b the crystal packing is presented. Additionally, in Figures 6a and b the two types of channels in the crystal structure of **4** are indicated. The important interatomic distances and angles are given in the Figure 5 caption. The list of metal-ligand bond lengths and metal-metal distances is given in the Table S1 of the ESI. The highest density Zn-*zni* phase obtained here, during the synthesis in water at RT, was earlier produced solvothermally as $Zn(Im)_2$ by Lehnert & Seel, (1980)[64] and as $Co(Im)_2$ by Tian et al. (2003).[25] Zn-*zni* of $Zn(Im)_2$ was also observed during the recrystallization of the melt above 400°C.[65]

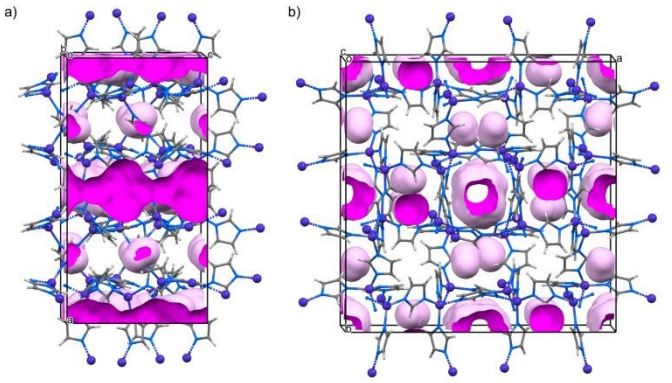


**Figure 6**. The voids/channels in the crystal structure of **4c**: a) viewed along axis *b*; b) viewed along axis *c*. The maximum radius of the larger channel is 2 Å.

The ratio of metals in the bimetallic samples of **4** was evaluated by the elemental analysis; carbon content was selected for the calculations (as the most reliable datum, Table 3). The experiments confirmed a variable ratio for **4a**-**4e** thus we can infer that Co is randomly distributed within Zn position as in similar systems described recently by Zhou and co-workers (2017).[30] We have calculated the molar ration of Zn and Co from the carbon content established by EA and it returned Zn:Co 8.1:1 for **4a** and 9.5:1 for **4b**. Similar calculations gave negative values for Co content in **4c** and **4e**. It must be observed that the cobalt mass percentage is low in samples **4a** to **4e**, with the highest recorded at about 3.6% in **4a**. Moreover, the molar masses of cobalt and zinc are closely aligned. Consequently, even minor experimental errors can render calculations unfeasible, as exemplified in the cases of **4c** and **4e**. The elemental analysis for **4d** reveals a higher cobalt content, deviating from the trend which must have been our experimental error.

Additionally, we scrutinized the morphology and metal ratios for the selected specimens of **4** using Energy Dispersive X-ray (EDX) analysis. The morphological characteristics of **4a** and **4c** are visually depicted in Figures 10a and b. SEM images confirm the presence of small homogeneous nanocrystals (rods) in the sample of **4a**, while the sample of **4c** is partly amorphous. The EDX analytical results are compiled in Table 5. The presented values were computed as the averages derived from measurements made, at least, on three different points of each sample. It is noteworthy that the standard deviation of the averaged values did not surpass 3%. The ratio of Zn:Co in **4a** is 7.59:1 – slightly lower than the same ratio obtained from elemental analysis (Zn:Co = 8.1:1). For **4c** the molar ratio Zn:Co is 9.05:1 (not accessible by elemental analysis) – thus the change is in accordance with the synthetic conditions. Both elemental analysis and EDX show that cobalt is over-represented in the material compared to the ratio of metals in solution. Together with the results of elemental analysis it suggests that phases containing more cobalt are more crystalline and stable.

**Table 5**. The ratio of metals in heterometallic samples from EDX experiments.

| Cmpd. No. | Zn [mol %] | Ag [mol %] | Co [mol %] | Expected ratio | Observed ratio |
|---|---|---|---|---|---|
| **4a** | 88.36± 0.215 | --- | 11.64± 0.215 | Zn:Co 9:1 | 7.59:1 |
| **4c** | 90.05± 1.483 | --- | 9.95± 1.483 | Zn:Co 11:1 | 9.05:1 |
| **5** | 27.47± 2.368 | 71.18± 2.744 | --- | Ag/Zn = 2/1 | Ag/Zn = 2.59/1 |
| **6** | --- | 60.55± 2.789 | 39.45± 2.789 | Ag/Co = 2/1 | Ag/Co = 1.53/1 |

Contrary to **4**, compounds **5** and **6** have a definite chemical composition $Ag_2M(Im)_4$ where in **5** M= Zn and in **6** M=Co. Both compounds, which are isostructural, crystallize in tetragonal crystal system, space group $P\text{-}42_1c$ with small differences in cell parameters: a=b=11.3668(3) Å, c=6.2738(4) Å, V= 810.42(4) Å for compound **5**, and a=b=11.3300(4) Å, c=6.2085(2) Å, V= 796.98(6) Å for compound **6**, both measured at RT (Figure 7, Tables 4 and 6). The molecular structures of **5** and **6** were solved *ab initio* by XRPD and the results of the Rietveld refinement are shown in Figures 8a and b.

View Article Online
DOI: 10.1039/D3DT03115

The sample of **6** studied by XRPD produced smaller average intensities than the sample of **5** and the larger background.

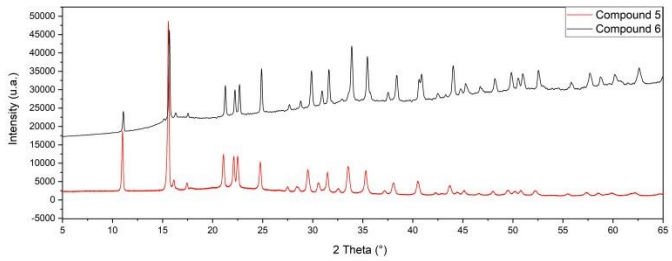


**Figure 7.** XRPD patterns for compounds **5** and **6** of the general formula $Ag_2MIm_4$, where M=Zn (**5**) or Co (**6**).

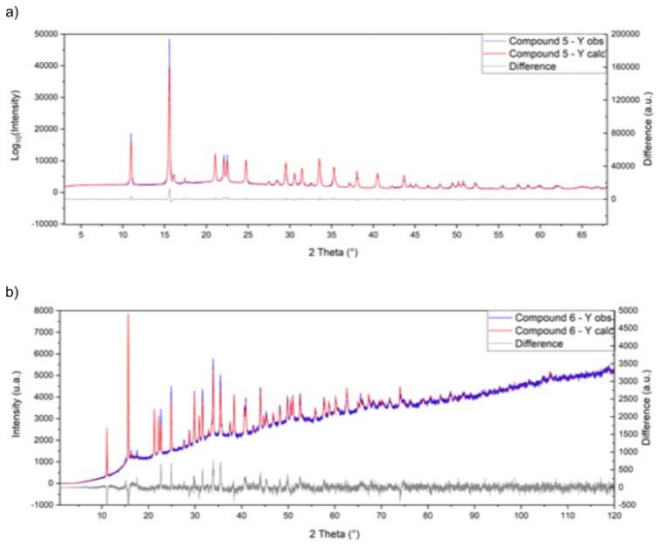


**Figure 8.** The results of the Rietveld refinement of: a) **5**; b) **6**.

The molecular structure and crystal packing of **5** are shown in Figure 9a-d and the molecular structure of **6** is the same, so we do not illustrate it separately. The asymmetric unit of **5** holds only 0.5 of silver atom, 0.25 of the zinc atom and one imidazole (Figure 9a). The silver atoms are located on proper 2-fold axes, while the zinc atoms sit on 4-fold rotoinversion axes. These symmetry elements result from typical coordination geometries of these metal ions, which they adopt in compound **5** (and **6**): linear for silver atoms (C.N. = 2) and tetrahedral for Zn and Co atoms (C.N. = 4) as illustrated in Figure 9b. Figures 9c and d show the crystal packing: the silver rods oriented along axis c (Figure 9c) as well a distorted arrangement of imidazolate moieties, and a less porous structure compared to **4** (Figure 9d). The Ag(I)···Ag(I) contacts within the rods are 3.136 Å in **5** and slightly shorter, namely 3.104 Å in **6**. Such Ag(I)···Ag(I) distances suggest a certain, fractional bond order.[66] For the list of metal–ligand bond lengths and a discussion on intermetallic contacts please refer to the Figure 9 and Table S2 of the ESI.

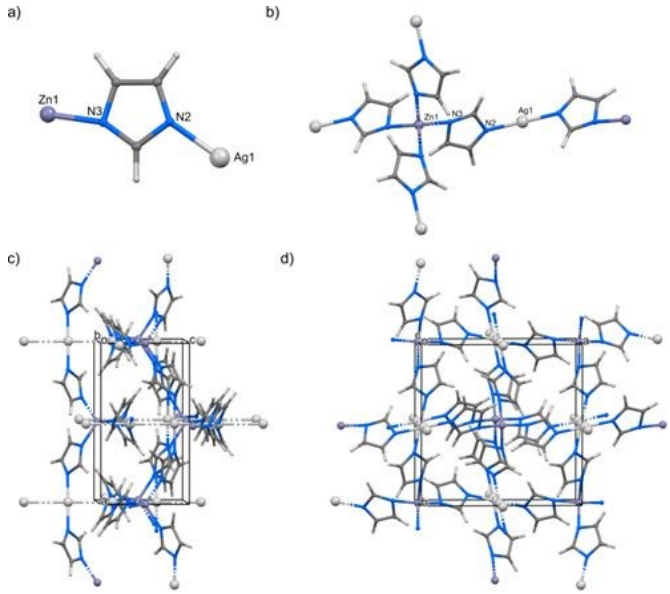


**Figure 9**. The molecular structure and crystal packing of **5**: a) independent unit; b) coordination environment of zinc(II) and silver(I); c) crystal packing viewed along axis b; d) crystal packing viewed along axis *c*. Bond lengths: Zn-N 2.049 Å; Ag-N 2.051 Å; Angles N-Zn-N 107.64°, 113.19°, N-Ag-N 178.67°.

The compounds **5** and **6** are isostructural with heterometallic Cu(I)/Zn[15,18] and Cu(I)/Co(II)[53] imidazolates; the unit cell parameters of all compounds are compared in Table 6 and metal ligand bond lengths for silver and copper imidazolates are collected in Table S2.[15,18,53] The metal-ligand bonds are definitely shorter for copper analogs, in accordance with the difference in the ionic radii of copper and silver. On the contrary, the Cu···Cu and Ag···Ag contacts are of comparable lengths, which indicates once more the existence of argentophilic interactions within the chains of silver atoms.

For more discussion on the characteristic crystal packing features of several transition metal imidazolates (described here and the literature data[1,28,29,67]), please refer to the ESI content including Table S3 and Figure S1.

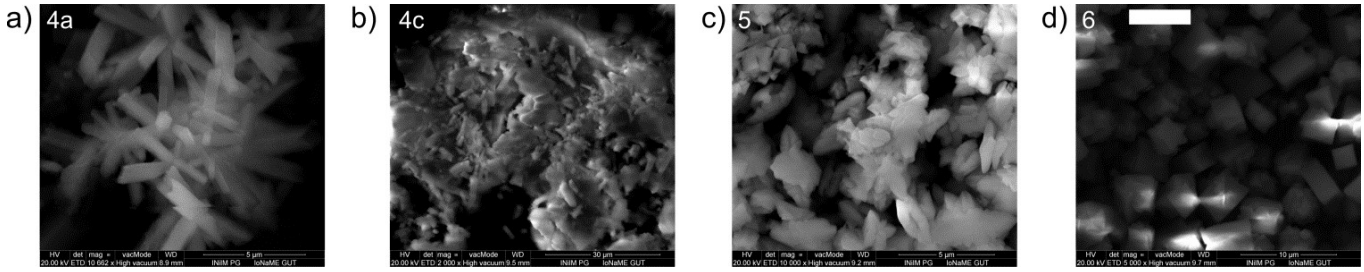


**Figure 10.** SEM images of compounds: a) **4a**; b) **4c**; c) **5** and d) **6**.

**Table 6**. The comparison of the unit cell parameters of **5** and **6** with the literature data for isostructural copper analogs.

View Article Online
DOI: 10.1039/D3DT03211F

| Compd. | Chemical formula | Crystal system/ Space group | a/Å | b/Å | c/Å | V/Å$^3$ | T/K | Ref. |
|---|---|---|---|---|---|---|---|---|
| **5** | $Ag_2Zn(N_2C_3H_3)_4$ | Tetragonal/P-42$_1$c | 11.3668(3) | 11.3668(3) | 6.27238(4) | 810.42(4) | 298 | This work |
| **6** | $Ag_2Co(N_2C_3H_3)_4$ | Tetragonal/P-42$_1$c | 11.3300(4) | 11.3300(4) | 6.2085(2) | 796.98(6) | 298 | This work |
| ZIF-202 | $Cu_2Zn(N_2C_3H_3)_4$ | Tetragonal/P-42$_1$c | 10.9623(3) | 10.9623(3) | 6.3231(4) | 759.86(6) | 298 | [15] |
| ZIF-202 | $Cu_2Zn(N_2C_3H_3)_4$ | Tetragonal/P-42$_1$c | 10.9562(4) | 10.9562(4) | 6.2181(2) | 746.41(6) | 100 | [18] |
| - | $Cu_2Co(N_2C_3H_3)_4$ | Tetragonal/P-42$_1$c | 10.9513(15) | 10.9513(15) | 6.3063(13) | 756.3(2) | 293 | [53] |

The elemental analyses for compounds **5** and **6** exhibit very satisfactory conformity with the anticipated formula (Table 3). Likewise, the morphology observed in the EDX images suggests a high degree of crystallinity and uniformity in the samples of **5** (rhombohedrons) and **6** (cubes) – see Figure 10c and d. However, the Ag:M molar ratio calculated from EDX data deviates from the anticipated value of 2:1, with a recorded value of 2.59:1 for sample of **5** and 1.53:1 for sample of **6** (Table 5). We attribute the deviation to systematic errors inherent in this analytical method.

### FTIR spectroscopy

The FTIR spectra of the imidazolates **1** – **6** are relatively simple and very similar. We have used the FTIR spectroscopy as the first indication of the purity of the obtained samples during the optimization of the synthesis of **1**. It also confirms the absence of water in the obtained solids. The FTIR spectra of pure imidazolates do not show the characteristic, very large and broad mode $\upsilon_{NH}$ of unreacted imidazole (Figure 11).

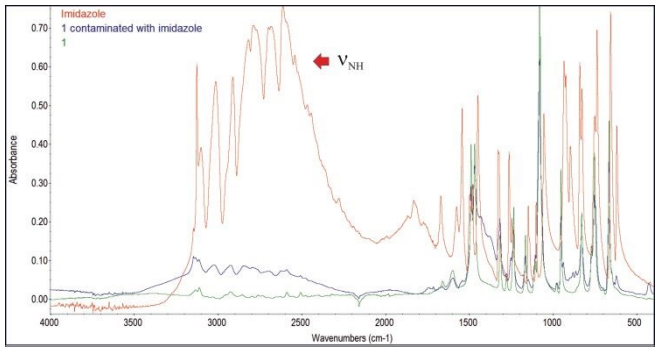


**Figure 11.** The FTIR spectra of **1** and imidazole.

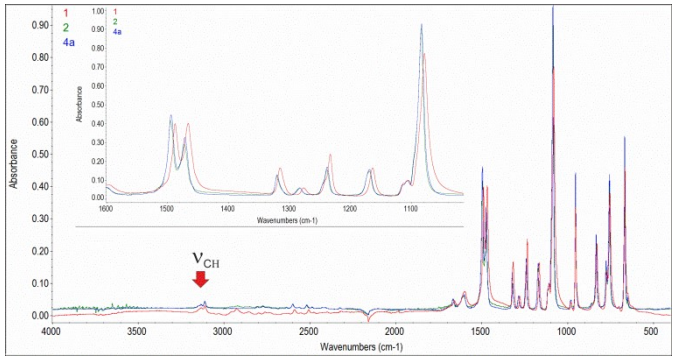


**Figure 12.** The FTIR spectra of **1**, **2**, and **4a**. The inset shows that there are some minor shifts in the fingerprint region of the spectra.

All FTIR spectra of imidazolates **1** – **6** are demonstrated in ESI as Figures S2-S11. The spectra of compounds **1** and **2** as well as the heterometallic **4** (represented by **4a**) are hardly distinguishable (Figure 12). The FTIR spectra of silver and silver-based heterometallic imidazolates **3**, **5** and **6** feature $\upsilon_{CH}$ mode of larger intensity, which is connected with the change in the coordination geometry – tetrahedral for Zn/Co imidazolates and linear for Ag containing imidazolates. This $\upsilon_{CH}$ mode is centered at approximately 3120 cm$^{-1}$ (Figure 13).

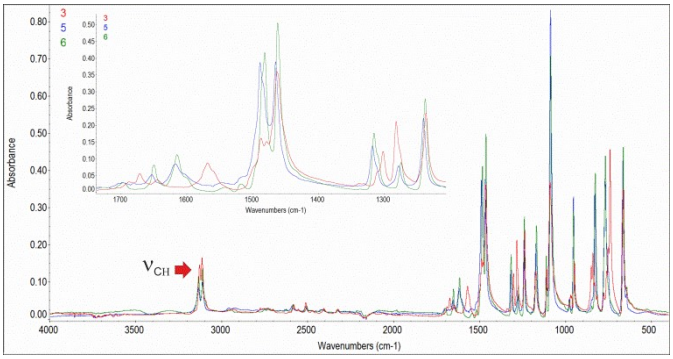


**Figure 13.** The FTIR spectra of **3**, **5**, and **6**. The inset shows some of the differences in the fingerprint region of the spectra.

### UV-Vis – optical absorption properties

The presence of an imidazole ring as a chromophore in combination with a transition group metal can result in π-π* and n-π* (47,650-37,750 cm$^{-1}$/209-265 nm) and LMCT (ligand-to-metal charge-transfer) (40,000-29,450 cm$^{-1}$/250-340 nm) interactions.[68-71] In the complexes of Co(II) ions the optical properties are mainly due to *d-d* transitions, between which relaxation and emission processes occur.[72]

The spectra of ideal tetrahedral Co(II) complexes usually consist of two bands present in the NIR and Vis regions. Frequently, splittings into three separate arms are encountered in the visible region. In this type of spectra, the following transitions can be distinguished: $^4A_2(F) \rightarrow {}^4T_1(F)$ (11,000 - 5,000cm$^{-1}$/909 - 2000), $^4A_2 \rightarrow {}^4T_1(P)$ (19,500 - 13,500 cm$^{-1}$/513 - 741 nm).[73,74] For compounds showing a square or distorted planar structure, we can distinguish transitions of the type: $^4T_{1g}(F) \rightarrow {}^4T_{2g}(F)$ (10,500 - 6,500 cm$^{-1}$/952 - 1538 nm) and $^4T_{1g}(F) \rightarrow {}^4T_{1g}(P)$ (22,000 - 15,500 cm$^{-1}$/455 - 645 nm).[75] Octahedral Co(II) complexes are characterized by bands present in the 525-575 nm range (19,048 - 17,391cm$^{-1}$) accompanied by $^4T_{1g}(F) \rightarrow {}^4T_{1g}(P)$ transitions. In addition, the transitions $^4T_{1g}(F) \rightarrow {}^4T_{2g}(F)$ (11,635 - 8811 cm$^{-1}$/859 - 1135 nm) and $^4T_{1g} \rightarrow {}^4A_{2g}(F)$ 1(16,447 - 3,550-cm$^{-1}$/608 - 2817 nm) are often visible in the near-infrared.[76,77]

The reflection spectra of complexes **1** - **6** (Figure 14a-d, Table 7) showed only slight differences in band offset, which indicate the presence of similar coordination or structural geometry.

View Article Online
DOI: 10.1039/D3DT03115E

**Table 7**. UV-Vis reflectance spectra.

| Compound | Absorption Maxima | | Assignments |
|---|---|---|---|
| | λ [nm] | ũ [cm$^{-1}$] | |
| **1** | 215.93 | 46 296 | π-π* |
| | 285.62 | 35 087 | $\pi_1$(imidazole) → Co(II) LMCT |
| | 537.83 | 18 622 | $^4A_2$→ $^4T_1$(P) |
| | 575.01 | 17 391 | |
| **2** | 218.58 | 45 662 | π-π* |
| | 302.21 | 33 112 | $\pi_1$ (imidazole) → Zn(II) LMCT |
| **3** | 207.35 | 48 309 | π-π* |
| | 249.26 | 40 161 | n-π* |
| | 297.99 | 33 557 | $\pi_1$ (imidazole) → Ag(I) LMCT |
| **4a** | 215.93 | 46 296 | π-π* |
| | 291.58 | 34 364 | $\pi_1$ (imidazole) → Co(II) LMCT |
| | 539.16 | 18 552 | $^4A_2$→ $^4T_1$(P) |
| | 571.68 | 17 482 | |
| **4b** | 213.95 | 46 729 | π-π* |
| | 292.74 | 34 247 | $\pi_1$ (imidazole) → Co(II) LMCT |
| | 537.17 | 18 622 | $^4A_2$→ $^4T_1$(P) |
| | 571.97 | 17483 | |
| **4c** | 215.27 | 46 512 | π-π* |
| | 291.59 | 34 247 | $\pi_1$ (imidazole) → Co(II) LMCT |
| | 537.51 | 18 484 | $^4A_2$→ $^4T_1$(P) |
| | 571.68 | 17 482 | |
| **4d** | 223.89 | 44 643 | π-π* |
| | 290.93 | 34 364 | $\pi_1$ (imidazole) → Co(II) LMCT |
| | 537.75 | 18 519 | $^4A_2$→ $^4T_1$(P) |
| | 571.78 | 17 482 | |
| **4e** | 218.58 | 45 662 | π-π* |
| | 291.78 | 34 247 | $\pi_1$ (imidazole) → Co(II) LMCT |
| | 537.98 | 18 692 | $^4A_2$→ $^4T_1$(P) |
| | 571.68 | 17 483 | |
| **5** | 217.26 | 46 083 | π-π*1 |
| | 219.21 | 45 662 | π-π*2 |
| | 239.82 | 41 667 | n-π* |
| | 297.57 | 33 557 | $\pi_1$ (imidazole) → Ag(I)/Zn(II) LMCT |
| **6** | 222.52 | 44 843 | π-π* |
| | 289.40 | 34 602 | $\pi_1$ (imidazole) → Co(II) LMCT |
| | 539.74 | 18 519 | $^4A_2$→ $^4T_1$(P) |
| | 571.52 | 17 483 | |

The electronic spectra of **1** and **4** in the solid state showed ligand-field bands in the range of 537-575 nm which consisted of Co(II) *d-d* transitions typical for ideal tetrahedral geometry. A major band can be distinguished at 571 nm with a shoulder band at about 537 nm. The UV range consists of characteristic bands at 213-223 nm, and 289-291nm which is attributed to π-π* and $\pi_1$ (imidazole) → Co(II) LMCT. A visible difference between the UV-Vis spectra of the compounds numbered **4a-e** was the different intensities of the bands, roughly in agreement with the synthetic conditions and molar ratio of zinc to cobalt in the reaction mixtures. The spectrum of compound **5** shows similarity to **2** and **3** and contains four bands at 217, 219, 240 and 298 nm. The solid-state spectrum of compound **6** is comparable to compound **1** and **4**, showing bands at around 223, 289, 540 and 572 nm.

On the basis of UV-Vis spectra we have calculated the HOMO-LUMO separations of all the materials. Two published procedures were applied.[78] With a reference to the recent work on $Co_xZn_{1-x}(2MeIm)_2$ [79] we can suggest that Co-doped ZIFs **4** feature a small excitation energy (a small band gap) of 1.96-2.0 eV, which may indicate a wide spectrum of responsive characteristics of the samples (please, refer to the ESI materials Figures S12-S17 and Tables S4 and S5). To verify these data and confirm the properties, transient photocurrent responses, Mott-Schottky curve and EIS spectra will be carried out in the future.

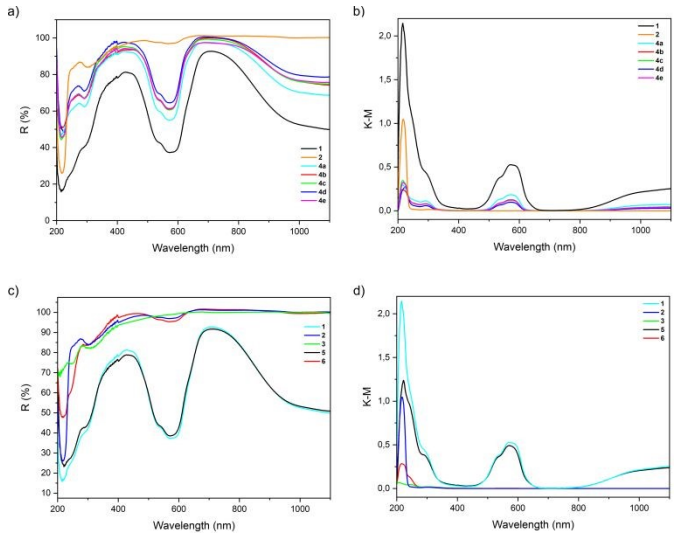


**Figure 14.** Solid-state electronic spectra of compounds **1** - **6**.

### Thermogravimetry of bimetallic imidazolates 4, 5, 6

Since the results of TG analysis for **1** - **3** were published by other authors,[2] we have only studied the thermal stability of bimetallic compounds. It was demonstrated that all tested compounds are characterized by high thermal stability in the air atmosphere. In Figure 15, a sharp weight loss was observed after exceeding 420 °C and 450 °C for compounds **4a** and **4c**, respectively. In the case of **4c**, the maximum rate of weight loss occurred at 480 °C (ESI, Figure S19.), while for **4a** (ESI Figure S18) it was shifted to 520 °C.

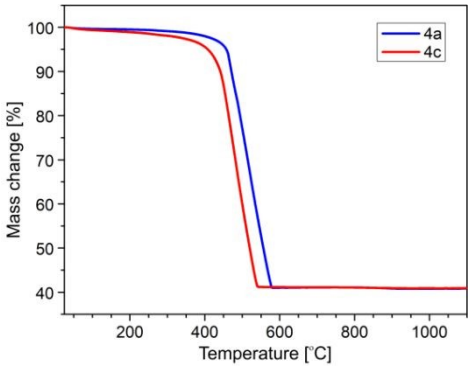


**Figure 15.** TG results for **4a** and **4c.**

The total weight loss was equal to 59.2% for compound **4a** and 59.1% for compound **4c**. Together with the green colour of the solid residue it corresponds to the removal of the organic part

View Article Online
DOI: 10.1039/D3DT03211F

and formation of a mixed-metal oxide in the presence of air (Riemann's green: ZnO·CoO).

As shown in Figure 16, compounds **5** and **6** have lower thermal stability compared to compounds **4a** and **4c**. In the case of compound **5**, after exceeding 240 °C, the TG curve begins to decline, with the highest weight loss rate at the temperature of 365 °C (ESI, Figure S20). For compound **6**, the weight loss occurs at the temperature of 320 °C, reaching the highest rate at the temperature close to that obtained for compound **5** - 370 °C (ESI, Figure S21).

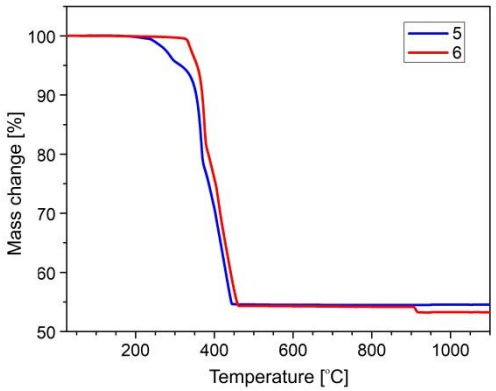


**Figure 16.** TG results for **5** and **6**.

In the case of compounds **5** and **6**, we can observe 3 zones of weight loss – 240–330 °C (5.9%), 330–375 °C (16.4%) and 375-445 °C (23.0%) for compound **5** and 320-350 °C (3.9%), 350-380 °C (14.9%) and 380-460 °C (26.9%) for compound **6**. In addition, for compound **6** a slight weight loss <1% was observed at 910 °C, which may correspond to the conversion of $Co_3O_4$ into CoO. The mass of the residue – 54.7% for **5** and 54.3% for **6** as well as metallic lustre of the residue correspond to the mixture of metallic silver and cobalt or zinc oxides. In the case of **5** the theoretical mass percentage of silver plus the respective metal oxide (Ag + ZnO) is 54.10% of the initial mass of the sample - experimental result for the residue is 54.7%. For **6** Ag plus $Co_3O_4$ would be equal to 54.57% of the initial mass of the sample and experiment returns 54.3%. Moreover, the decomposition of $Co_3O_4$ into CoO corresponds to the further weight loss of 1.17%, which is observed in the TG plot. The suggested numbers are in very good agreement with the experimental results.

**Catalysis: oxidation of phenylethanol to acetophenone in the presence of bimetallic metal imidazolates**

To assess the catalytic activity of heterometallic imidazolates **4-6** in the oxidation of organic compounds, we repeated the procedure described previously.[62] The reaction between *tert*-butyl peroxide and 1-phenylethanol:

$$t\text{BuOOH} + \text{PhCH(OH)CH}_3 \rightarrow t\text{BuOH} + \text{PhC(O)CH}_3 + \text{H}_2\text{O}$$

practically does not proceed without the addition of the catalyst in the applied conditions, which was confirmed independently in all experiments (Figure 15). The reactions were performed in the presence of suspended complexes in catalytic amounts of 0.0145 g or 0.029 g , which is *ca.* 0.75/1.5 mol% for **4e** and *ca.* 0.5/1.0 mol% for **5** and **6**.

Out of the three studied materials only one exhibited certain catalytic activity and it was compound **6** (Figure 17). At the temperature of 80 °C during the 2 hours of the reaction it helped to convert approximately 20% or the substrate into the oxidation product. Without the catalyst the reaction was completed only in 5%. We confirmed this result in several experiments that included the variable temperature attempts (40, 60 and 80 °C – for compounds **5** and **6**) and evaluation over time (2 and 6 hrs. for compound **6**). The additional results are presented in ESI as Figures S22-S24. With compound **6** at 40 °C the yield of the catalyzed reaction is low but raising the temperature from 60 to 80 °C does not enhance the yield to a significant extent, thus 60 °C should be recommended. The elongation of reaction time from 2 to 6 hrs at 80 °C allows to increase the yield to approximately 40% (with the yield of control reaction at approximately 10%). Complex **6** was recovered from the reaction mixture by filtration and found to be intact by FTIR ATR analysis. The double amount of catalyst had little influence on the reaction yield (compare Figure 17 and Figure S23).

We were initially convinced that the presence of silver ions should be enough to secure the activity of the complex in the reaction of oxidation because silver ions are used as a catalyst of oxidation in similar systems.[80] Thus we expected that **5** will demonstrate similar catalytic activity to **6**, but it was not the case. Probably the concerted action of Co and Ag is needed to accelerate the reaction. We would also like to mention the recent results of Xu et. al. (2023)[79] that indicate the important influence of irradiation onto the catalytic activity of similar compounds. So far we have carried out the experiments in dark.

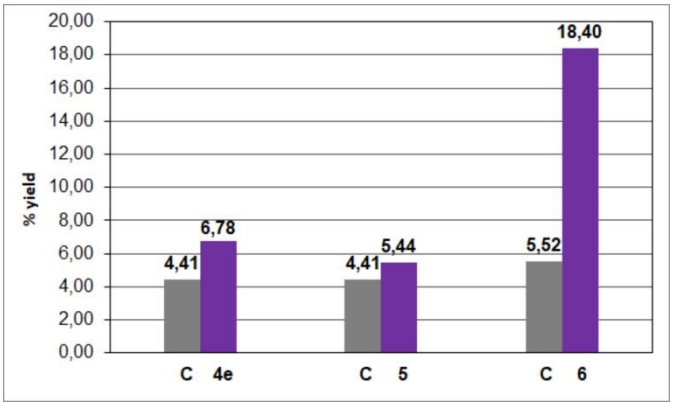


**Figure 17**. Influence of the addition of complexes **4e**, **5** and **6** onto the yield of the reaction between the *tert*-butyl peroxide and 1-phenylethanol. Each sample with the individual control; **C**, reaction without the addition of the complex, **4e**, **5**, **6** – the yield of the reaction with the addition of 0.0145 g of the given complex per 0.605 ml pf 1-phenylethanol (see Experimental). The experiment performed at 80 °C.

## Conclusions

A series of mono and bimetallic imidazolates of Co, Zn and Ag was produced by a very simple synthetic approach in water as a solvent with little energy consumption. The proposed approach enables the production of these materials within a short time frame, emphasizing both simplicity and speed. Additionally, it features the limited use of energy for heating. Because of the use of water instead of harmful solvents this synthetic approach represents a step towards the

exploitation of green chemistry processes. By the described method nanocrystalline powders are obtained. FTIR spectroscopy proved to be a useful tool that may quickly help to identify and evaluate the purity of the obtained imidazolates. The crystal structures of bimetallic imidazolates $Co_xZn_{(1-x)}Im_2$ (**4a-e**), $Ag_2ZnIm_4$ (**5**) $Ag_2CoIm_4$ (**6**) were examined by powder diffraction. Cobalt imidazolate **1** as well as heterometallic Co/Zn imidazolates showed the standard ZIF-8 crystal structure. EDX experiments as well as elemental analysis indicate that above ~2.8% w/w of cobalt in Zn/Co imidazolates, which corresponds to about 9-10 mol% of metal atoms, the samples are very pure and crystalline. With less cobalt the obtained phases become more amorphous. Ag insertion together with Zn or Co gives a more compact structure analogous to the Cu(I) – Co/Zn bimetallic imidazolates. All discussed imidazolates feature certain common motives in the solid state. The thermal stability of bimetallic **4** is very good and resembles that of monometallic zinc and cobalt imidazolates.[2] Zn/Ag and Co/Ag imidazolates **5** and **6** start to decompose in much lower temperatures of 240 and 320 °C respectively. The preliminary catalytic experiments indicated that out of the studied heterometallic compounds only $Ag_2Co(Im)_4$, exhibits significant catalytic activity in the reaction of oxidation of 1-phenylethanol by *tert*-butylhydroxyperoxide at elevated temperature. Further experiments are needed to confirm the small band gaps of the cobalt imidazolates and catalytic activity of the Co-containing materials upon irradiation with the visible light.

## Author Contributions

Mattia Lopresti – PXRD measurements and structure solution – bimetallic compounds, Łukasz Kurowski – synthesis of bimentallic imidazolates, catalytic experiments, Luca Palin - SEM,EDX experiments, Marco Milanesio – PXRD measurements, structure solution, writing the manuscript, Magdalena Siedzielnik – FTIR measurements, Karolina Gutmańska – UV-Vis measurements, writing manuscript, Adriana Dobrenko – synthesis of monometallic imidazolates, Tomasz Klimczuk – PXRD measurements and interpretation– monometallic compounds, EDX measurements, Ewelina Pawelczyk – synthesis of monometallic imidazolates, TG experiments, Anna Dołęga – conceptualization, writing and editing the manuscript.

## Conflicts of interest

There are no conflicts to declare.

## Acknowledgements

Ms. Martina Basilicata and Mr. Szymon Piekarski are acknowledged for their synthetic work. A.D., K.G., M.S., A.D. and Ł.K. thank the Gdańsk Tech Core Research Facilities DEC-5/2021/RES for providing the PerkinElmer Lambda 365+ double-beam UV/Vis spectrometer with an integrating sphere for measurements.

## Notes and references

1 Y.-Q. Tian, C.-X. Cai, Y. Ji, X.-Z. You, S.-M. Peng and G.-H. Lee, *Angew. Chem. Int. Ed.*, 2002, **41**, 1384.
2 K. S. Park, Z. Ni , A. P. Côté , J. Yong Choi , R. Huang, F. J. Uribe-Romo , H. K. Chae , M. O'Keeffe and O. M. Yaghi, *Proc. Natl. Acad. Sci.*, 2006, **103**, 10186.
3 The Cambridge Structural Database: C. R. Groom, I. J. Bruno, M. P. Lightfoot and S. C. Ward, *Acta Crystallogr. B*, 2016, **B72**, 171.
4 E. C. Spencer, R J. Angel, N. L. Ross, B. E. Hanson and J. A. K. Howard, *J. Am. Chem. Soc.*, 2009, **131**, 4022.
5 T. D. Bennett, P. Simoncic, S. A. Moggach, F. Gozzo, P. Macchi, D. A. Keen, J.-Chong Tan and A. K. Cheetham, *Chem. Commun.*, 2011, **47**, 7983.
6 I. E. Collings, A. B. Cairns, A. L. Thompson, J. E. Parker, C. C. Tang, M. G. Tucker, J. Catafesta, C. Levelut, J. Haines, V. Dmitriev, P. Pattison and A. L. Goodwin, *J. Am. Chem. Soc.* 2013, **135**, 7610.
7 R. N. Widmer, G. I. Lampronti, S. Chibani, C. W. Wilson, S. Anzellini, S. Farsang, A. K. Kleppe, N. P. M. Casati, S. G. MacLeod, S. A. T. Redfern, F.-X. Coudert and T. D. Bennett, *J. Am. Chem. Soc.*, 2019, **141**, 9330.
8 C. A. Schröder, I. A. Baburin, L. van Wüllen, Michael Wiebcke and S. Leoni, *CrystEngComm*, 2013, **15**, 4036.
9 M. T. Wharmby, S. Henke, T. D. Bennett, S. R. Bajpe, I. Schwedler, S. P. Thompson, F. Gozzo, P. Simoncic, C. Mellot-Draznieks, H. Tao and Y. Yue, *Angew. Chem. Int. Ed.*, 2015, **54**, 6447.
10 R. Gaillac, P. Pullumbi and F. X. Coudert, *J. Phys. Chem. C*, 2018, **122**, 6730.
11 L. Frentzel-Beyme, M. Kloß, R. Pallach, S Salamon, H. Moldenhauer, J. Landers, H. Wende, J. Debus and S. Henke, *J. Mater. Chem. A*, 2019a, **7**, 985.
12 L. Frentzel-Beyme, M. Kloß, P. Kolodzeiski, R. Pallach and S. Henke, *J. Am. Chem. Soc.*, 2019b, **141**, 12362.
13 J. Hou, M L. Ríos Gómez, A. Krajnc, A. McCaul, S. Li, A. M. Bumstead, A. F. Sapnik, Z. Deng, R. Lin, P. A. Chater, D. S. Keeble, D. A. Keen, D. Appadoo, B. Chan, V. Chen, G. Mali and T. D. Bennett, *J. Am. Chem. Soc.*, 2020, **142**, 3880.
14 M. L. Ríos Gómez, G. I. Lampronti, Y. Yang, J. C. Maurod and T. D. Bennett, *Dalton Trans.*, 2020, **49**, 850.
15 D. M. Schubert, M. Z. Visi and C. B. Knobler, *Inorg. Chim. Acta*, 2009, **362**, 4832.
16 O. Karagiaridi, M. B. Lalonde, W. Bury, A. A. Sarjeant, O. K. Farha and J. T. Hupp, *J. Am. Chem. Soc.*, 2012, **134**, 18790.
17 E. A. Flügel, V. W.-h. Lau, H. Schlomberg, R. Glaum and B. V. Lotsch, *Chem. Eur. J.* 2016, **22**, 3676.
18 N. T. T. Nguyen,T. N. H. Lo, J. Kim, H. T. D. Nguyen, T. B. Le, K. E. Cordova and H. Furukawa, *Inorg. Chem.*, 2016, **55**, 6201.
19 Y. Tian, B. Mu, B. Li, X. Li, W. Xu and Y. Lin, *ChemistrySelect*, 2019, **4**, 3841.
20 S. Cong, Q. Shen, M. Shan, J. Wang, J. Liu and Y. Zhang, *Chem. Eng. J.*, 2020, **383**, 123137.
21 Y. Lin, Q. Zhang, C. Zhao, H. Li, C. Kong, C. Shen and L. Chen, *Chem. Commun.*, 2015, **51**, 697.
22 K. Müller-Buschbaum, S. Gomez-Torres, P. Larsen and C. Wickleder, *Chem. Mater.*, 2007, **19**, 655.
23 J.-C. Rybak, M. Hailmann, P. R. Matthes, A. Zurawski, J. Nitsch, A. Steffen, J. G. Heck, C. Feldmann, S. Götzendörfer, J. Meinhardt, G. Sextl, H. Kohlmann, S. J. Sedlmaier, W. Schnick and K. Müller-Buschbaum, *J. Am. Chem. Soc.*, 2013, **135**, 6896.
24 L. V. Meyer, F. Schönfeld, A. Zurawski, M. Mai, C. Feldmann and K. Müller-Buschbaum, *Dalton Trans.*, 2015, **44**, 4070.
25 Y.-Q. Tian, C.-X. Cai, X.-M. Ren, C.-Y. Duan, Y. Xu, S. Gao and X.-Z. You, *Chem. Eur. J.* 2003, **9**, 5673.
26 B. Shen, B. Wang, L. Zhu and L. Jiang, *Nanomaterials*, 2020, **10**, 1636.
27 J. Song, R. Pallach, L. Frentzel-Beyme, P. Kolodzeiski, G.

Kieslich, P. Vervoorts, C. L. Hobday and S. Henke, *Angew. Chem. Int. Ed.*, 2022, **61**, e202117565.
28 N. Masciocchi, F. Castelli, P. M. Forster, M. M. Tafoya and A. K. Cheetham, *Inorg. Chem.*, 2003, **42**, 6147.
29 R. Banerjee, A. Phan, B. Wang, C. Knobler, H. Furukawa, M. O'Keeffe and O. M. Yaghi, *Science*, 2008, **319**, 939.
30 K. Zhou, B. Mousavi, Z. Luo, S. Phatanasri, S. Chaemchuen and F. Verpoort, *J. Mater. Chem. A*, 2017, **5**, 952.
31 A. M. Bumstead, M. L. Ríos Gómez, M. F. Thorne, A. F. Sapnik, L. Longley, J. M. Tuffnell, D. S. Keeble, D. A. Keen and T. D. Bennett, *CrystEngComm*, 2020, **22**, 3627.
32 S. Guo, H.-Z. Li, Z.-W. Wang, Z.-Y. Zhu, S.-H. Zhang, F. Wang and J. Zhang, *Inorg. Chem. Front.*, 2022, **9**, 2011.
33 I. R. Speight, I. Huskić, M. Arhangelskis, H. M. Titi, R. S. Stein, T. P. Hanusa and T. Friščić, *Chem. Eur. J.*, 2020, **26**, 1811.
34 N. Masciocchi, M. Moret, P. Cairati, A. Sironi, G. A. Ardizzoia and G. La Monica, *J. Chem. Soc., Dalton Trans.*, 1995, 1671.
35 J. A. J. Jarvis and A. F. Wells, *Acta Crystallogr.* 1960, **13**, 1027.
36 N. Masciocchi, S. Bruni, E. Cariati, F. Cariati, S. Galli and A. Sironi, *Inorg. Chem.*, 2001, **40**, 5897.
37 Y.-Q. Tian, Y.-M. Zhao, Z.-X. Chen, G.-N. Zhang, L.-H. Weng and D.-Y. Zhao, *Chem. Eur. J.*, 2007, **13**, 4146.
38 Q.-Q. Meng, J. Wang, Q. Shi and J.-X. Dong, *CrystEngComm*, 2021, **23**, 3429.
39 Q. Shi, W.-J. Xu, R.-K. Huang, W.-X. Zhang, Y. Li, P.-F. Wang, F.-N. Shi, L. Li, J.-P. Li and J.-X. Dong, *J. Am. Chem. Soc.*, 2016, **138**, 16232.
40 D. M. Schubert, D. T. Natan and C. B. Knobler, *Main Group Chem.*, 2008, **7**, 311.
41 Y.-Q. Tian, Z.-X. Chen, L.-H. Weng, H.-B. Guo, S. Gao and D. Y. Zhao, *Inorg. Chem.*, 2004a, **43**, 4631.
42 T. Wu, X.-H. Bu, J. Zhang and P.-Y. Feng, *Chem. Mater.*, 2008, **20**, 7377.
43 S. Chen, J. Zhang, T. Wu, P. Feng and X. Bu, *Dalton Trans.*, 2010, **39**, 697.
44 G. A. V. Martins, P. J. Byrne, P. Allan, S. J. Teat, A. M. Z. Slawin, Y. Li and R. E. Morris, *Dalton Trans.*, 2010, **39**, 1758.
45 S. Burazer, F. Morelle, Y. Filinchuk, R. Černý and J. Popović, *Inorg. Chem.*, 2019, **58**, 6927.
46 A. Zurawski, F. Hintze and K. Müller-Buschbaum, *Z. Anorg. Allg. Chem.* 2010, **636**, 1333.
47 K. Müller-Buschbaum and F. Schönfeld, *Z. Anorg. Allg. Chem.*, 2011, **637**, 955.
48 A. Zurawski, J.-C. Rybak, L. V. Meyer, P. R. Matthes, V. Stepanenko, N. Dannenbauer, F. Würthner and K. Müller-Buschbaum, *Dalton Trans.*, 2012, **41**, 4067.
49 P. J. Beldon, L. Fábián, R. S. Stein, A. Thirumurugan, A. K. Cheetham and T. Friščić, *Angew. Chem., Int. Ed.*, 2010, **49**, 9640.
50 M. F. Thorne, M.L. Ríos Gómez, A. M. Bumstead, S.-C. Li and T. D. Bennett, *Green Chem.*, 2020, **22**, 2505.
51 I. Brekalo, C. M. Kane, A. N. Ley, J. R. Ramirez, T. Friščić and K. T. Holman, *J. Am. Chem. Soc.*, 2018, **140**, 10104.
52 A. Zurawski, M. Mai, D. Baumann, C. Feldmann and K. Müller-Buschbaum, *Chem. Commun.*, 2011, **47**, 496.
53 Y.-Q. Tian, H.-J. Xu, Y.-Z. Li and X.-Z. You, *Z. Anorg. Allg. Chem.*, 2004b, **630**, 1371.
54 X.-C. Huang, J.-P. Zhang, Y.-Y. Lin, X.-L. Yua and X.-M. Chen, *Chem. Commun.*, 2004, 1100.
55 J.-P. Zhang and X.-M. Chen, *Chem. Commun.*, 2006, 1689.
56 M. Ahmad, M. Yousaf, W. Cai and Z.-P. Zhao, *Chem. Eng. J.*, 2023, **453**, 139846.
57 X.-C. Huang, J.-P. Zhang and X.-M. Chen, *Chin. Sci. Bull.*, 2003, **48**, 1531.
58 G. Ivarsson, B. K. S. Lundberg and N. Ingri, *Acta Chem. Scand.*, 1972, **26**, 3005.
59 B. K. S. Lundberg, *Acta Chem. Scand.*, 1972, **26**, 3902.
60 S. Zheng, T. Wu, J. Zhang, M. Chow, R. A. Nieto, P. Feng and X. Bu, *Angew. Chem. Int. Ed.* 2010, **49**, 5362.
61 W. M. Haynes, (ed.). CRC Handbook of Chemistry and Physics. 95th Edition. CRC Press LLC, Boca Raton: FL 2014-2015, p. 3-84.
62 A. Mielcarek, A. Bieńko, P. Saramak, J. Jezierska and A. Dołęga, *Dalton Trans.*, 2019, **48**, 17780.
63 S. Landi, I. R. Segundo, E. Freitas, M. Vasilevskiy, J. Carneiro, C. J. Tavares, *Solid State Commun.*, 2022, **341**, 114573, doi: 10.1016/j.ssc.2021.114573.
64 R. Lehnert and F. Seel, *Z. anorg. allg. Chem.*, 1980, **464**, 187.
65 T. D. Bennett, A. L. Goodwin, M. T. Dove, D. A. Keen, M. G. Tucker, E. R. Barney, A. K. Soper, E. G. Bithell, J.-C. Tan and A. K. Cheetham, *Phys. Rev. Lett.,* 2010, **104**, 115503.
66 H. Schmidbaur and A. Schier, *Angew. Chem. Int. Ed.,* 2015, **54**, 746.
67 X.-C. Huang, J.-P. Zhang, X.-M. Chen, *Cryst. Growth Des.*, 2006, **6**, 1194.
68 E. Bernarducci, P. K. Bharadwaj, K. Krogh-Jespersen, J. A Potenza and H. J. Schugar, *J. Am. Chem. Soc.*, 1983, **105**, 3860.
69 A. Dołęga, A. Pladzyk, K. Baranowska and J. Jezierska, *Inorg. Chim. Acta*, 2009, **362**, 5085.
70 A. Fudulu, R. Olar, C. Maxim, G.V. Scăeţeanu, C. Bleotu, L. Matei and M. Badea, *Molecules*, 2020, **26**, 55.
71 Richa, N. Kumar, J. Sindhu, Y. Patil, S. K. Sharma, B. Pani and R. Kataria, *Inorg. Chem. Commun.*, 2020, **122**, 108280.
72 V. Sivo, G. D'Abrosca, L. Russo, R. Iacovino, P. V. Pedone, R. Fattorusso and G. Malgieri, *Bioinorg. Chem. Appl.*, 2017, **2017**, 1527247.
73 L. Banci, A. Bencini, C. Benelli, D. Gatteschi and C. Zanchini, *Struct. Bond.*, 2007, **52**, 37.
74 D. Kowalkowska-Zedler, A. Dołęga, N. Nedelko, R. Łyszczek, P. Aleshkevych, I. Demchenko and A. Pladzyk, *Dalton Trans.*, 2020, **49**, 697.
75 R. Reshma, R Selwin Joseyphus, D. Arish, R. J. Reshmi Jaya and J. Johnson, *J. Biomol. Struct. Dyn.*, 2022, **40**, 8602.
76 A. P. Mishra, R. K. Mishra, M. D. Pandey, *Russ. J. Inorg. Chem.*, 2011, **56**, 1757.
77 M. Gulcan, Y. Karataş, S. Işık, *J. Fluoresc.* 2014, **24**, 1679.
78 P. Makuła, M. Pacia, W. Macyk, J. Phys. Chem. Lett., 2018, **9**, 6814.
79 D. Xu, X. Yu, X. Jiang, J. Zhang, Z. Ni, M. Wang, Catal. Commun., 2023, **185**, 106810.
80 H. A. Ewais, A. S. Basaleh, Y. M. Al Angari, *Int. J. Chem. Kinet.* 2023, **55**, 271.